JOURNAL OF AIRCRAFT
Vol. 48, No. 3, May–June 2011

Flow Control of Tiltrotor Unmanned-Aerial-Vehicle Airfoils Using Synthetic Jets

Minhee Kim,* Sanghoon Kim,† Woore Kim,† and Chongam Kim‡
Seoul National University, Seoul 151-742, Republic of Korea
and
Yushin Kim§
Korea Aerospace Research Institute, Daejeon 305-333, Republic of Korea

DOI: 10.2514/1.C031225

Flow control using synthetic jets has been computationally investigated to improve aerodynamic performance of tiltrotor unmanned-aerial-vehicle airfoils under various flight conditions. Many features of complex tiltrotor flows were captured, including wing leading-edge and trailing-edge separation and the massive region of separated flow beneath the wing. To control the separation of the leading and trailing edges in hovering and transition-flight modes, synthetic jets were located at suitable positions ($0.01c$, $0.3c_{\text{flap}}$, and $0.95c_{\text{flap}}$). It was observed that the flow structure and rate of drag reduction could be substantially improved, depending on the frequency of synthetic jets in hovering mode. Based on the flow control results in hovering mode, separation control was performed at transition mode. Detailed computations revealed the download could be efficiently reduced by using both the leading-edge and trailing-edge jets in hovering flight mode, and the leading-edge jet only in transition-flight modes. This indicates that the flight performance of tiltrotor unmanned aerial vehicles could be remarkably improved by applying an active flow control strategy based on synthetic jets.

Nomenclature

A_{jet}	=	suction or blowing amplitude, instantaneous peak velocity at orifice
c	=	chord length
C_μ	=	momentum coefficient, $(A_{\text{jet}}/U_\infty)^2 h/c$
c_f	=	chord length of flap, $c_f/c = 0.31$
f	=	frequency of periodic excitation
$F+$	=	nondimensional frequency, fc_f/U_∞
h	=	slot width
U_∞	=	freestream velocity

I. Introduction

A TILTROTOR unmanned aerial vehicle (UAV) is a unique flight vehicle that combines the vertical takeoff and landing capability of the helicopter with the efficient high-speed cruise performance of the conventional fixed-wing aircraft. This is achieved, among others, by positioning, at the wingtips of a fixed wing, a rotor that can be tilted so as to provide lift for hover and thrust for cruise flight. However, tiltrotor configuration must overcome adverse aerodynamic download in hover that is caused by the drag induced from the rotor downwash. The rotor downwash results in separated flow on the downstream side of the wing, and the download brings a significant penalty in the payload or vertical lift capability. Because the rotor flow hits the wing in hover, the download force on the wing has been measured to be about 10–15% of the total rotor thrust [1]. Therefore, download alleviation is quite important for increasing the flight performance and payload capacity of such aircraft.

Received 3 September 2010; accepted for publication 4 January 2011.

*Ph.D. Candidate, Interdisciplinary Program in Computational Science and Technology.
†Ph.D. Candidate, Department of Aerospace Engineering.
‡Professor, Department of Aerospace Engineering; chongam@snu.ac.kr. Senior Member AIAA (Corresponding Author).
§Senior Researcher, Smart UAV Development Center.

Many researchers and engineers have studied download reduction using passive flow control. A flight test of XV-15 by Maisel and Harris [2] has provided quantitative estimates of hover performance including the effect of flap deflection angle on download. By increasing the flap deflection angle, the download can be reduced owing to the reduction in the effective wing area influenced by the rotor downwash as well as the reduction of the vertical drag coefficient. McCroskey et al. found that the drag on the airfoil during hover was sensitive to the flap angle and the surface-curvature distribution along the upper surface near the leading edge [3]. Further discussions on the effects of the wing geometry on the download can be found in research by Felker [4].

The capability of download alleviation can be provided by active flow control too. The effectiveness of active flow control was successfully demonstrated on a full-scale XV-15 aircraft. The reduction of the wing download was experimentally explored at NASA Ames Research Center [5,6]. The wing download was reduced by as much as 25–54% with continuous blowing slots [7]. In the experiment by Kjellgren et al., an oscillatory jet at the flap shoulder of a V-22 tiltrotor wing yielded a reduction of up to 40% of the download [8]. The effect of a thin tangential jet located at the wing leading edge of a tiltrotor configuration in hover was computed by Fejtek and Roberts using the thin-layer Navier–Stokes equations [9], which demonstrated the effectiveness of leading-edge tangential blowing in reducing the rotor download. The wing download of the V-22 tiltrotor aircraft using synthetic jets has also been studied by detached-eddy simulations [10].

Thus far, most studies about the alleviation of the tiltrotor download have focused on the hovering flight mode. To maintain a required level of thrust, however, download reduction is also necessary in transition flight mode as well as in hovering. Keeping this in mind, active flow control has been computationally conducted using synthetic jets for download reduction in hovering and transition flight modes.

A synthetic jet is one of the most actively studied flow control devices, because it has a potential to be implemented in actual aircraft flow control system. Many researchers and engineers produced impressive experimental and numerical studies. Vasile et al. [11] and Vaccaro et al. [12] experimentally investigated the flow structures and interactions caused by a synthetic jet over a finite and sweptback wing and inside inlet ducts. Kim and Kim [13] and Kim et al. [14] studied flow control mechanisms of synthetic jets using a

NACA 23012 airfoil and the effect of jet exit configuration on flow control performance. The flowfield of a round synthetic jet issuing into a crossflow was investigated by Xia and Mohseni [15], and a synthetic jet was applied for low-speed maneuvering and station-keeping of small underwater vehicles [16]. Chaudhari et al. studied the effects of excitation frequency, cavity design, and orifice shape [17,18]. Zhou and Zhong obtained the interaction of a circular synthetic jet with boundary layer, and they examined the formation and development of coherent structures using the Q criterion [19,20]. In addition, research on the interaction between synthetic jets with crossflow was conducted experimentally and numerically by Wood et al. [21]. Günther et al. [22] and Petz and Nitsche [23] studied flap separation control by periodic excitation near the flap for high-lift configuration.

The focus of the present paper is to control the separated flow around the tiltrotor smart UAV (SUAV) airfoil in hovering and transition flight modes. The SUAV is the unmanned Korean tiltrotor aircraft that has vertical takeoff and landing capability with a high-speed cruise performance. To achieve the goal, the flow structures over the SUAV airfoil in hovering and transition flight modes were first investigated. Based on the observed flow structures, leading-edge and trailing-edge separation flows were controlled using synthetic jets. First, synthetic jets were applied to the leading and trailing edges in hovering flight mode. Since the actual flow control mechanism and flow structure can be fundamentally different, depending on synthetic jet parameters [13], flow characteristics were examined according to the jet location and nondimensional jet frequency. Efficient synthetic jets were then employed to reduce the download on the leading and trailing edges. Second, separation flow control was conducted in transition flight modes based on the flow control results in hovering. Finally, by comparing the flow control results of synthetic jets located at the leading and trailing edges, the most effective flow control condition was obtained at hovering and transition flight modes.

II. Numerical Methods

A. Governing Equations

Accurate prediction of stall characteristics, with or without turbulence models, is still an extremely challenging task. By considering available computing power and required numerical accuracy, the present approach relies on solving unsteady Reynolds-averaged Navier–Stokes (URANS) equations. A URANS simulation combined with adequate turbulence models, such as the κ-ω shear stress transport (SST) turbulence model, can provide reasonably good solutions [24].

The incompressible governing equations are given by the continuity equation and the momentum equation for the conservation of mass and momentum, where the overbar indicates a Reynolds-averaged quantity:

$$\nabla \cdot \bar{u} = 0 \tag{1}$$

$$\rho \frac{\partial \bar{u}}{\partial t} + \rho \bar{u} \cdot \nabla \bar{u} = -\nabla \bar{p} + (\mu + \mu_t)\nabla^2 \bar{u} \tag{2}$$

The governing equations were then solved in a time-accurate manner by employing the method of pseudocompressibility, where τ is the pseudotime and β is the pseudocompressibility parameter [25,26]:

$$\frac{\partial \bar{p}}{\partial \tau} = -\beta \nabla \cdot \bar{u} \tag{3}$$

The upwind-differencing scheme based on flux-difference splitting, combined with the MUSCL approach, was used to calculate the convective term with a third-order spatial accuracy. The viscous fluxes were then centrally differenced by a second-order spatial accuracy, and the flow variables were updated by the lower–upper symmetric Gauss–Seidel time integration [27].

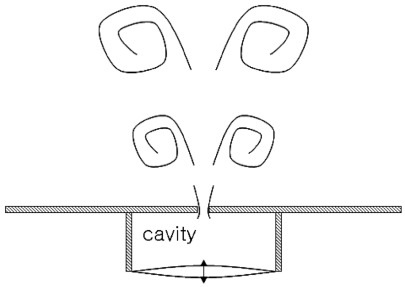

Fig. 1 Schematic of synthetic jet.

The turbulence model used in the present computation is the Menter SST two-equation model, which has provided excellent predictions of flows involving separation [26,28]. Also, the total stress limitation (TSL) method was employed to include the effect of flow transition [29]. All computations were performed with a finite volume-based in-house code that had been extensively validated [13,26,30].

B. Synthetic Jet Boundary Conditions

A synthetic jet actuator is an oscillatory jet generator that requires zero-net mass input yet produces a nonzero momentum output. Figure 1 shows a schematic of a synthetic jet actuator that contains an enclosed cavity with a small orifice on one face. At the Computational Fluid Dynamics (CFD) Validation Workshop at the second AIAA Flow Control Conference, Rumsey et al. reported that, compared with experiment data, the velocity distributions near the orifice exit might exhibit some anomalies neither captured nor modeled by CFD, but they also mentioned that global flow features could be captured with reasonably good accuracy [24,31].

Based on these results, the suction/blowing-type boundary condition proposed by Kral et al. [32], as in Eq. (4), was applied to the synthetic jet actuator. The top-hat condition, wherein the spatial variation of the jet at the orifice was neglected, was employed to obtain computationally efficient results without compromising physical reality [33]. A perturbation to the flowfield was then introduced by the jet velocity, where ξ denotes the streamwise direction, η denotes the cross-slot direction, $\mathbf{u}_n$ is a velocity vector, and $\mathbf{d}_{\text{jet}}$ is a unit vector in the jet direction:

$$\mathbf{u}_n(\xi = 0, \eta, t) = A_{\text{jet}} f(\eta) \sin(\omega t)\mathbf{d}_{\text{jet}}, \qquad f(\eta) = 1 \tag{4}$$

Figure 2 shows the computed centerline velocities compared with experimental data, which are measured using hot-wire anemometry along the cross-slot direction. The origin of the coordinate system is located at the center of the jet orifice. Except for some differences observed near the jet entrance, the computed results are in fair to good

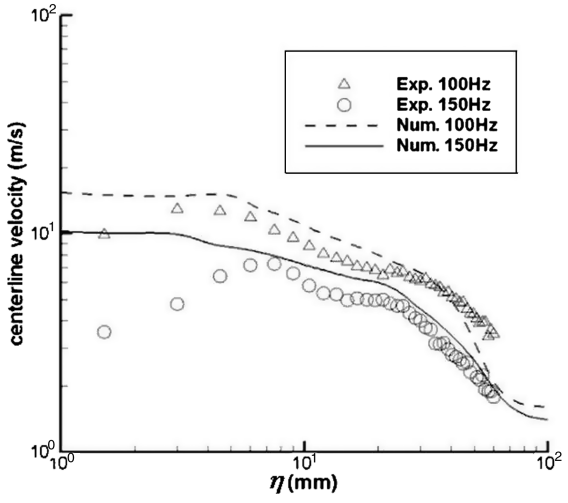

Fig. 2 Centerline velocity profile.

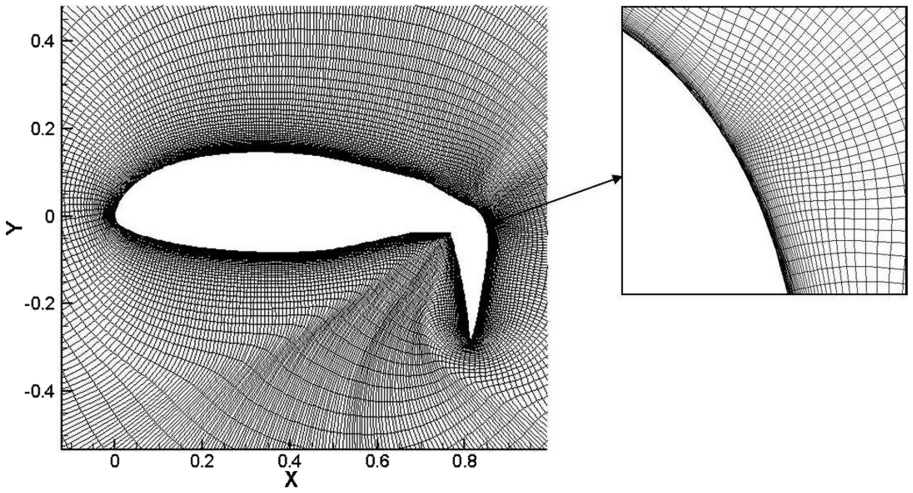

Fig. 3 Mesh for V-22 Bell A821801 airfoil.

agreement. It appears that the difference between computed and experimental results near the jet entrance is mainly due to the velocity fluctuation caused by hot-wire anemometry near the jet entrance [34].

III. Code Validation

The case of the V-22 Bell A821801 airfoil with a flap deflection angle of 85° was considered for code validation. The geometric details and experimental data can be found in [10]. The chord Reynolds number is 3×10^5, the angle of attack is $-85°$, and the velocity of the downstream rotor is 17 m/s. The synthetic jet is located at a flap chord length of 0.3 with the slot width of 0.2% of the flap chord length, and its angle with the surface tangent is 32°. The nondimensional frequency $F+$ is 0.6, and the momentum coefficient C_μ is 0.011. The boundary conditions of Eq. (4) can be determined from $F+$ and C_μ.

Figure 3 shows the V-22 Bell A821801 airfoil mesh and close-up view of the jet-slot region. A hyperbolic O grid was used with the wall spacing of a 1.0×10^{-5} chord. The outer boundary was extended to 25 chords. The number of grid points covering the jet slot was eight. To examine the grid sensitivity, three grid densities (509×120, 409×115, and 309×110) were considered for the noncontrolled and controlled cases. From the comparison of the computed results depicted in Fig. 4a, the differences between 509×120 and 409×115 are less than 2%, which is thought to be adequate for reliable computations. Thus, the 409×115 grid was chosen for code validation.

Table 1 Comparison of drag coefficients

	C_d
Experiments	1.49
k-ω SST with TSL	1.501
k-ω SST	1.253
Laminar	1.990

Using the chosen grid system, the time-step sensitivity was also examined. To maintain sufficient temporal accuracy, subiterations were conducted in pseudotime until the maximum flow divergence of the converged solution at the fixed physical time was less than 1.0×10^{-6}. Three levels of different time steps were tested: 40, 80, and 120 steps per synthetic jet period. Figure 4b shows the results of the pressure distribution against the number of time steps. The computational differences between 80 and 120 time steps were less than 2%, indicating that 80 time steps could adequately resolve the time-dependent nature of the flowfields within the URANS formulation. Computed results were obtained after reaching a sufficient level of time-periodic behavior.

Figure 4c shows the distribution of the time-averaged pressure coefficients along the chord length. Depending on the turbulence model and computations, some deviations between the computed results and experimental data can be observed. Since the flow region contains both laminar and turbulent flow dynamics, computational predictions using the κ-ω SST turbulent model combined with the TSL yield a reasonable agreement with experimental measurements. This is also confirmed from the results of Table 1. Although the computed results do not exactly agree with the experiment data, they do predict the general trend fairly accurately.

IV. Flow Control Results

The whole results are divided into two parts: analysis of flow structures and flow control over the SUAV airfoil using synthetic jets. The objective of the first part is to understand the basic flow features around the SUAV airfoil in hovering and transition flight modes. In the second part, for reducing the download by the rotor downwash that acts upon the wing, flow control using synthetic jets is simulated. The SUAV airfoil is composed of main airfoil and trailing-edge flap. The results are obtained using the overset grid method. Alhough not presented here, the choice of the overset grid system and time step was based on the resolution study, as in the case of the code validation.

Table 2 Flight conditions

Flight mode	Tilt angle, deg	Flap angle, deg	Freestream velocity, m/s	Reynolds number
Hovering	90	70	17	9.0×10^5
Transition 1	90	50	23.80	1.2×10^6
Transition 2	80	25	40.66	2.1×10^6
Transition 3	60	25	54.91	2.9×10^6
Transition 4	45	25	58.62	3.1×10^6
Transition 5	30	25	62.36	3.3×10^6
Transition 6	15	25	66.38	3.5×10^6

A. Basic Flow Structures over Smart Unmanned-Aerial-Vehicle Airfoil

As shown in Table 2, the flow structures over the SUAV airfoil were analyzed based on actual flight conditions. The standard flight condition of the SUAV was described in [35]. The induced velocity was obtained through the momentum theory by applying SUAV real disk loading. The freestream velocity and angle of attack were determined by the sum of the forward flight speed and the induced downwash velocity.

Figure 5 shows the drag histories according to the flight conditions. From now on, all of the horizontal axes of the drag histories indicate the nondimensional time scaled by the freestream

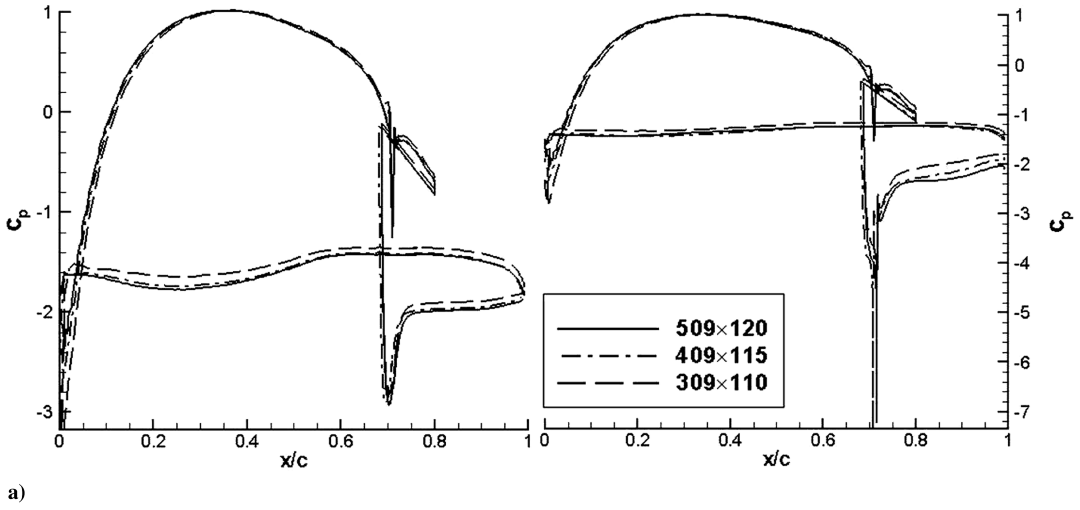

a)

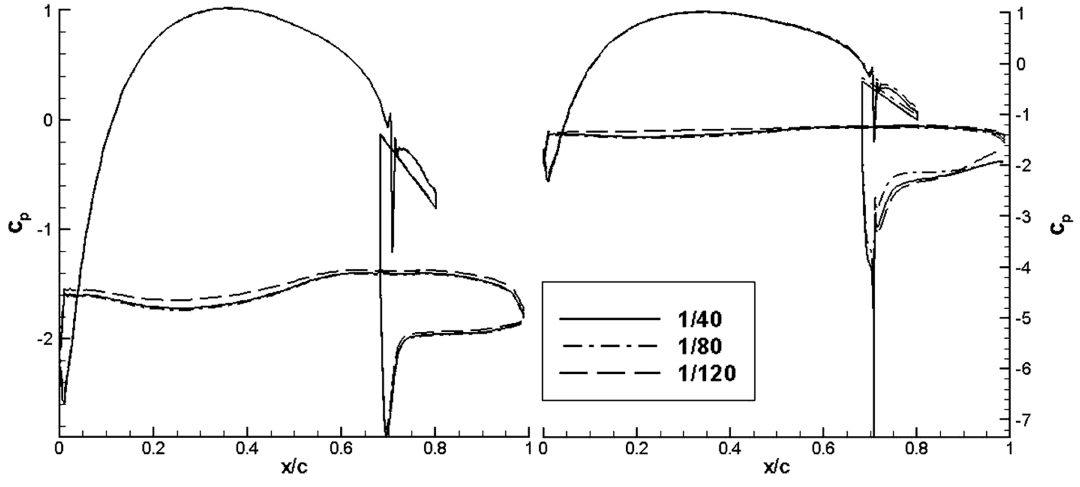

b)

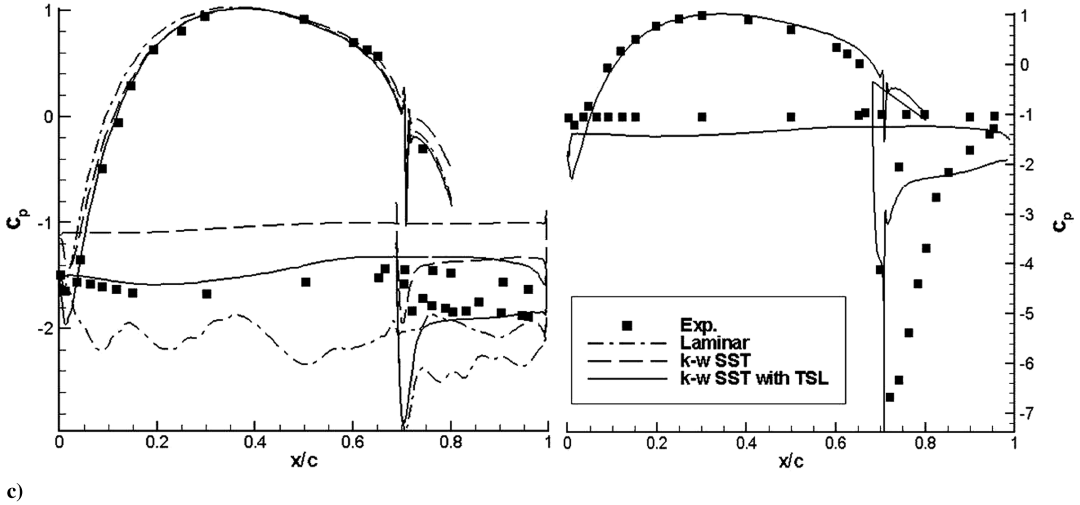

c)

Fig. 4 Comparison of pressure distributions (left: control off; right: control on): a) computational grids, b) time steps, and c) turbulence models.

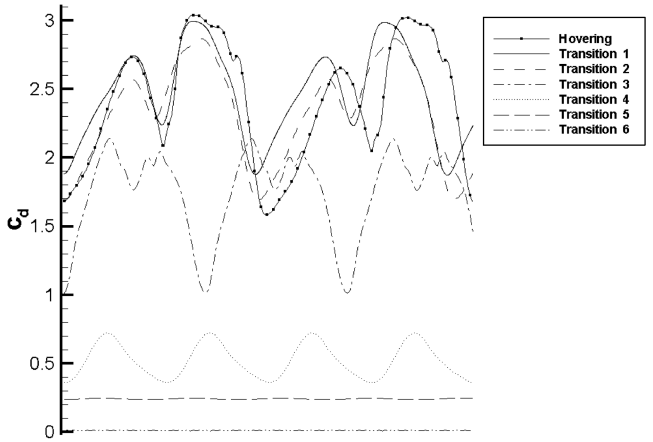

Fig. 5 Drag histories in hovering and transition flight modes.

velocity and the chord length of the SUAV airfoil. Drag refers to the force acting in the direction of the freestream velocity, and the wing download is caused by the drag force. Thus, the drag histories indicate the variation of the wing download. The drag histories show a regular periodicity, and their values increase as the direction of the tilt angle approaches 90°, as shown in Fig. 5. Since the flow is not separated in transition flight mode 6, in Table 2, flow structures are observed in hovering and transition flight modes 1–5.

Figure 6 shows some periodic patterns of drag histories and corresponding flow structures (or patterns of streamlines) in hovering flight mode. The overall flow pattern is as follows. For interval 1, the separated flow developed near the leading edge is attached on the lower surface of the airfoil and, as a result, a low-pressure region steadily grows. This leads to the monotonic increase in drag, which reaches the drag peak at the end of interval 1. For interval 2, the large leading-edge separation vortex, which is steadily increased by the rotor downwash, is finally detached from the lower surface, and it moves along the freestream direction. The drag is thus monotonically decreased. For interval 3, as the size of the vortex developed from the flap trailing edge becomes larger, the drag bounces back and grows

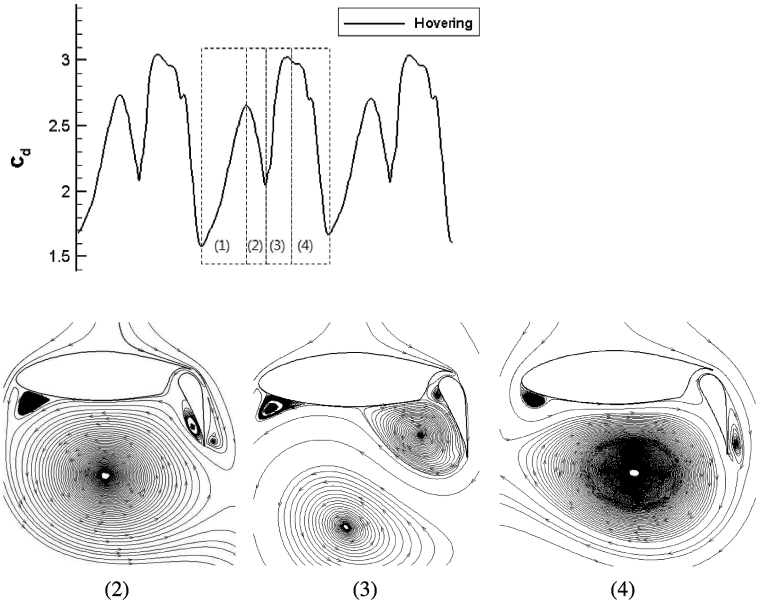

(1) (2) (3) (4)

Fig. 6 Flow pattern according to drag history in hover.

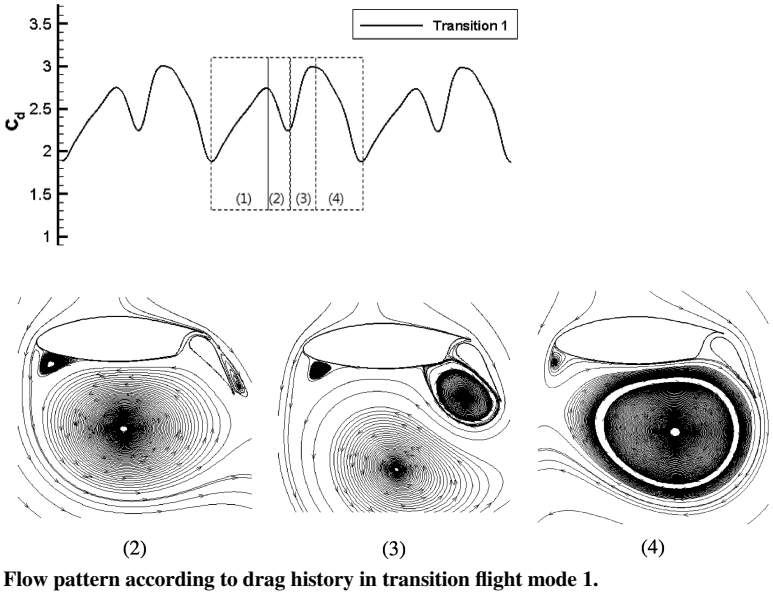

(1) (2) (3) (4)

Fig. 7 Flow pattern according to drag history in transition flight mode 1.

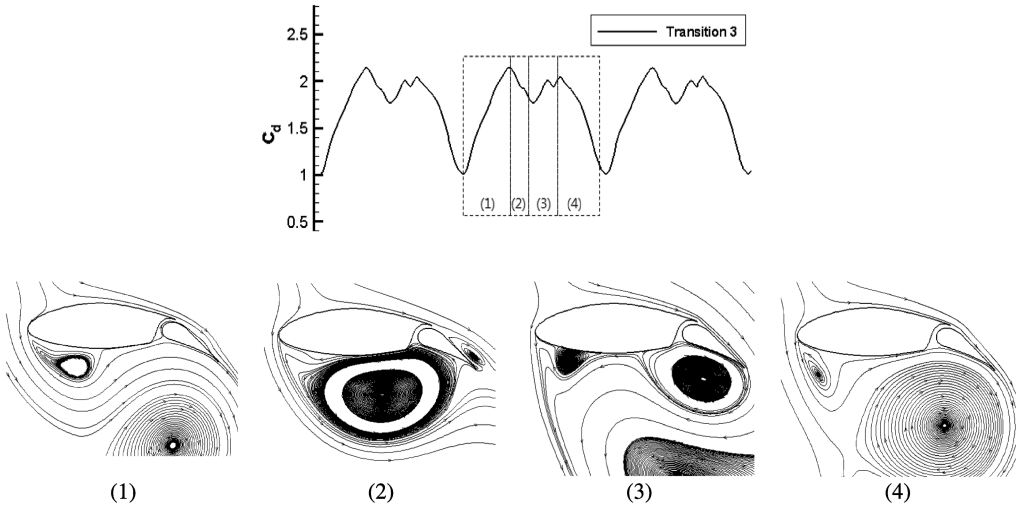

Fig. 8 Flow pattern according to drag history in transition flight mode 3.

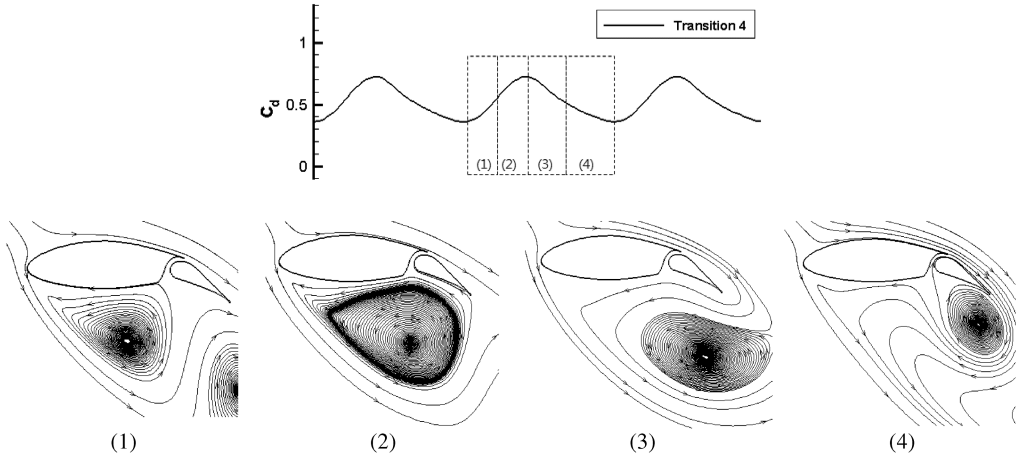

Fig. 9 Flow pattern according to drag history in transition flight mode 4.

again. For interval 4, the flap trailing-edge separation vortex is eventually detached from the lower surface, and the drag is decreased again. Overall, the wing download is alternatively fluctuated by the growth and detachment of the separation vortices at the leading and trailing edges.

The flow structures of transition flight modes 1 and 2 are similar to those of the hovering flight mode. The drag history and the change of the flow pattern of transition flight mode 1 are shown in Fig. 7. In intervals 1 and 2, drag changes depend on the growth and detachment of the leading-edge separation vortex. In intervals 3 and 4, a similar drag pattern can be observed according to the behavior of the flap trailing-edge separation vortex.

The flight condition of transition flight mode 3 is a tilt angle of 60° and a flap angle of 25°. In comparison with Figs. 7 and 8, it displays a somewhat different fluctuation pattern. The drag peak at the end of interval 1 is higher than the one observed at the end of interval 3. Like the case of transition flight mode 1, the drag peak is determined by the intensity of the leading-edge and flap trailing-edge separation vortices. As the tilt and flap angles become smaller, the horizontal component of the freestream velocity becomes larger and the vortex intensity is decreased. Compared with transition flight mode 1, the flap trailing-edge vortex is particularly less developed than the leading-edge vortex. As the flight mode changes from hovering to transition, this trend becomes clearer and the wing download is more

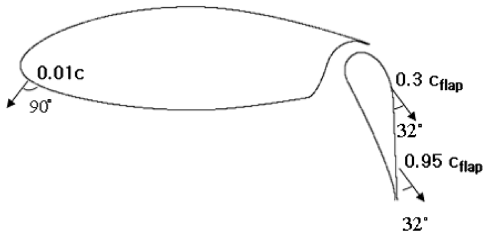

Fig. 10 Geometry of SUAV airfoil with synthetic jets.

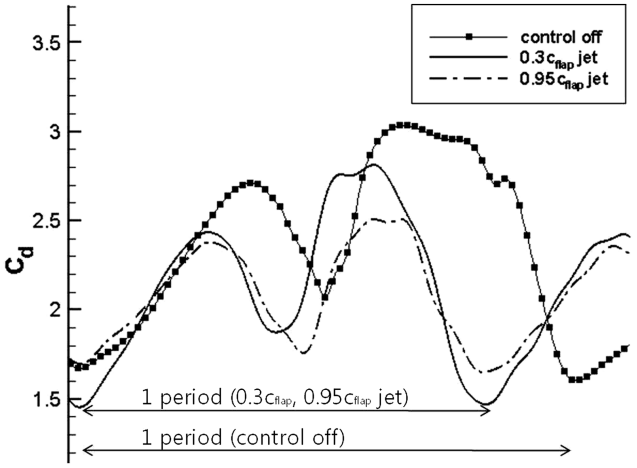

Fig. 11 Drag histories under trailing-edge flow control in hover ($F+ = 1$).

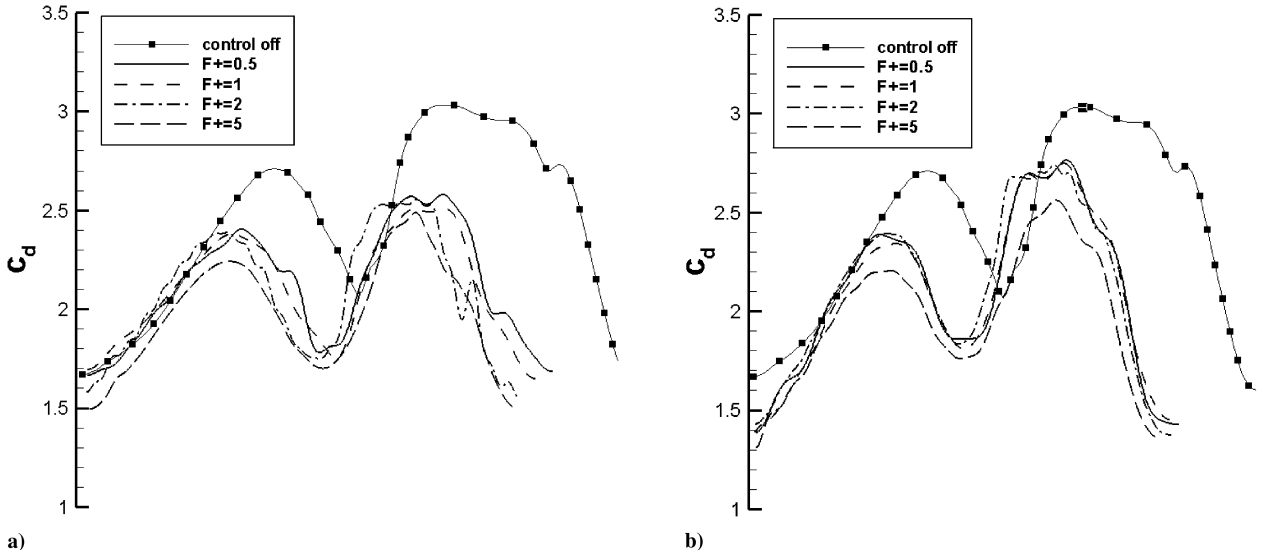

Fig. 12 Drag histories under trailing-edge flow control in hover ($F+ = 0.5$, 1, 2, and 5). (a) $0.95c_{\text{flap}}$ jet; (b) $0.3c_{\text{flap}}$ jet.

susceptible to the leading-edge vortex than the flap trailing-edge vortex. Hence, to suppress the wing download in the transition flight modes, the control of the leading-edge separation vortex is more important.

Transition flight mode 4 has a tilt angle of 45° and a flap angle of 25°. Figure 9 shows the drag pattern and flow structure. As the horizontal component of the freestream velocity becomes larger, the duration of the leading-edge vortex get longer, and the drag is continuously increased in intervals 1 and 2. At the end of interval 2, the leading-edge separation vortex is detached and the drag is reduced in interval 3. In interval 4, the flap trailing-edge separation vortex is created, but it is not attached to the flap lower surface; thus, the wing download is not increased. Overall, the drag history is solely determined by the growth and detachment of the leading-edge separation vortex. The drag pattern of transition flight mode 5 is quite similar to mode 4, except that the period becomes shorter, and the trailing-edge vortex is now developed on the flap upper surface.

Through an analysis of computed flowfields in the hovering and transition flight modes, it is observed that the wing download is determined by the growth and detachment of the leading-edge and flap trailing-edge vortices. In the hovering flight mode, the leading-edge and flap trailing-edge vortices are equally influential. In the transition flight modes, the role of the leading-edge vortex becomes more decisive. Exploiting the observed flow characteristics, leading-edge and trailing-edge separation controls are carried out to reduce the wing download.

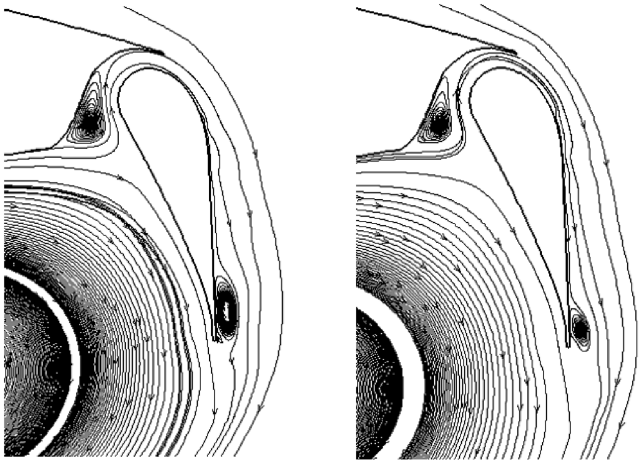

Fig. 13 Close-up view of streamlines at blowing/suction peak ($0.3c_{\text{flap}}$ jet, $F+ = 5$, left: blowing peak, right: suction peak).

B. Flow Control over Smart Unmanned-Aerial-Vehicle Airfoil

The geometry of the SUAV airfoil with synthetic jets, for leading-edge and trailing-edge separation control, is shown in Fig. 10. The leading-edge synthetic jet was located at 1% chord from the leading edge and is denoted as the $0.01c$ jet. Vortices produced by the $0.01c$ jet with a jet angle of 90° are going to change the structure of the leading-edge separation vortex. The trailing-edge synthetic jets were located at 30% flap chord and 95% flap chord, and they are denoted as the $0.3c_{\text{flap}}$ jet and $0.95c_{\text{flap}}$ jet, respectively. It is generally known that the effect of the synthetic jet is most visible when the jet location and the separation point are the same. Hence, the $0.3c_{\text{flap}}$ jet was near the separation point in the flap upper surface. In addition, the flows on the flap upper surface greatly contribute to the formation of the trailing-edge separation vortex below the flap. Thus, the $0.95c_{\text{flap}}$ jet was placed at the end of the trailing-edge flap to control the vortex formation. The inclination angle of the synthetic jets in the trailing edge was the same (32°) as the validation case. The peak jet velocity was 80 m/s in the hovering and transition flight conditions, which is within a range of feasible velocity [36,37]. The locations and jet angles of the synthetic jets were fixed in all flight modes. The drag histories were then analyzed using a low-path filter of the fast Fourier transform.

1. *Flow Control in Hovering Flight Mode*

Numerical simulations were performed by changing the major control parameters of the synthetic jet: the jet location and the

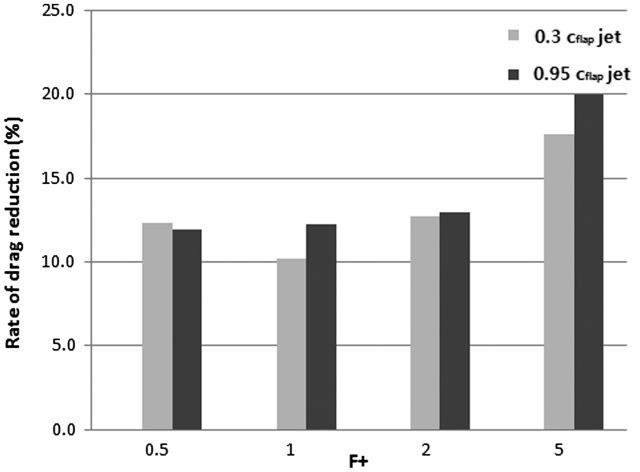

Fig. 14 Rate of drag reduction in terms of nondimensional frequency (flow control in hover; left: $0.3c_{\text{flap}}$ jet; right: $0.95c_{\text{flap}}$ jet).

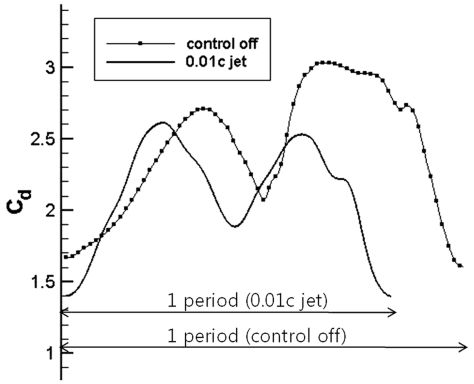

Fig. 15 Drag histories under leading-edge flow control in hover (0.01c jet, $F+ = 1$).

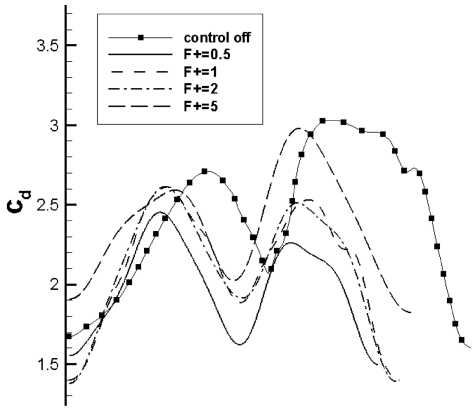

Fig. 17 Drag histories under leading-edge flow control in hover (0.01c jet; $F+ = 0.5$, 1, 2, and 5).

nondimensional frequency $F+$ of 0.5–5. The control parameters for locations $0.01c$, $0.3c_{\text{flap}}$, and $0.95c_{\text{flap}}$ are $F+ = 0.5$, 1, 2, and 5. The characteristic length used in the nondimensional frequency is the chord length of the trailing-edge flap.

a. Trailing-Edge Separation Control. The separation flow around the flap trailing edge was controlled by the synthetic jets located at $0.3c_{\text{flap}}$ and $0.95c_{\text{flap}}$. Figure 11 shows the drag histories with $F+ = 1$. From the suppression of the first drag peak, it is observed that the control of the trailing-edge vortex also affects the growth and detachment of the leading-edge separation vortex. From the basic flow features over the SUAV airfoil (Sec. IV.A), the growth and detachment of the leading-edge and flap trailing-edge vortices appear consecutively and periodically. The suppression of the flap trailing-edge vortex naturally shortens the time to develop and detach the leading-edge vortex, which results in the suppression of the first drag peak. It is interesting to observe in Fig. 11 that the $0.95c_{\text{flap}}$ jet performs better than the $0.3c_{\text{flap}}$ jet, particularly at the second drag peak. This indicates that the flows near trailing edge are critical in determining the intensity of the flap trailing-edge vortex, and the $0.95c_{\text{flap}}$ jet controls the trailing-edge flow feature more effectively.

Figure 12a shows the drag histories in terms of the nondimensional frequency ($F+ = 0.5$, 1, 2, and 5) with the $0.95c_{\text{flap}}$ jet. As the jet frequency increases, the period of the drag fluctuation becomes shorter. Thus, the high-frequency $0.95c_{\text{flap}}$ jet can effectively reduce the drag due to the trailing-edge separation vortex. The results with the $0.3c_{\text{flap}}$ jet in Fig. 12b exhibit a similar trend. Figure 13 shows the flow feature with a high-frequency $0.3c_{\text{flap}}$ jet, confirming again that, with a high-frequency synthetic jet, the flow near the synthetic jet slot tends to be firmly attached and, as a result, more stable flow structure can be obtained on the flap surface [13]. From the comparison of the drag histories between the $0.3c_{\text{flap}}$ jet with $F+ = 5$ and the $0.95c_{\text{flap}}$ jet with $F+ = 1$, one can see that the second drag peaks due to the trailing-edge separation vortex are almost identical, indicating that the $0.95c_{\text{flap}}$ jet with $F+ = 1$ gives the same performance as (and is thus more efficient than) the $0.3c_{\text{flap}}$ jet with $F+ = 5$. Finally, Fig. 14 shows the rate of drag reduction of the two jets in terms of jet frequency. The download can be reduced up to about 20% with a synthetic jet of $F+ = 5$. Overall, the $0.95c_{\text{flap}}$ jet located near the trailing edge turns out to be more effective than the $0.3c_{\text{flap}}$ jet located near separation point.

b. Leading-Edge Separation Control. Flow separation at the leading edge was controlled by the $0.01c$ jet. Figure 15 shows the drag histories when the nondimensional jet frequency is one. Basic flow control characteristics are quite similar to the case of trailing-edge separation control. First, the leading-edge synthetic jet suppresses the formation of the leading-edge separation vortex. The vortices produced by the $0.01c$ jet continuously disturb the large leading-edge separation vortex and finally split it into small vortices, as shown in Fig. 16. As the same time, the jet vortices push the small vortices and prevent them from staying longer at the airfoil lower surface, which leads to the suppression of the first drag peak. Second, the control of the leading-edge vortex positively interferes with the attachment and detachment of the trailing-edge separation vortex, leading to the substantial reduction of the second drag peak. As shown in Fig. 17, the drag peaks become lower and the period of the drag fluctuation tends to be shorter as the nondimensional jet frequency decreases. Particularly, the second drag peak is significantly suppressed in the case of lower jet frequency. The reason can be understood from Fig. 18. By a bigger vortex created by a lower-frequency jet, the flow structure at the airfoil lower surface is changed much more substantially. In addition, the suppression of the large leading-edge vortex favorably affects the detachment of the flap trailing-edge separation vortex. It is seen that the flow control effect is most visible with the leading-edge jet of $F+ = 0.5$.

The periodic behavior of the drag histories and flow structures in the case of $F+ = 0.5$ are shown in Fig. 19. For interval 1, the leading-edge synthetic jet alters the flow structures at the bottom of the airfoil. It splits the single leading-edge separation vortex into

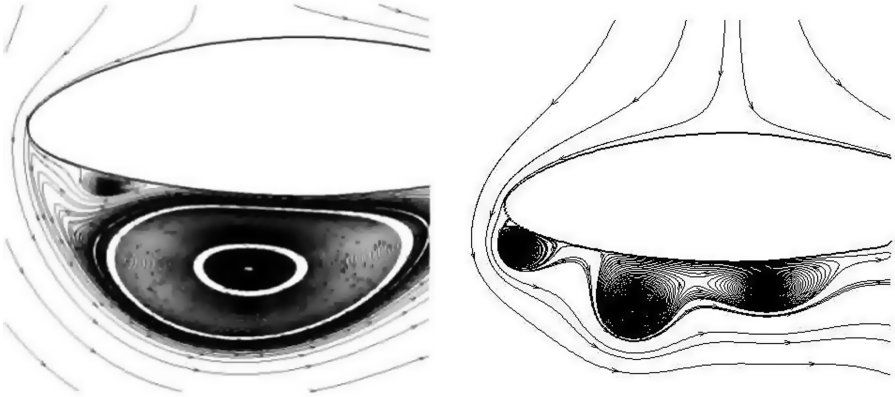

Fig. 16 Close-up view of streamlines of SUAV leading edge (0.01c jet, $F+ = 1$; left: control off; right: control on).

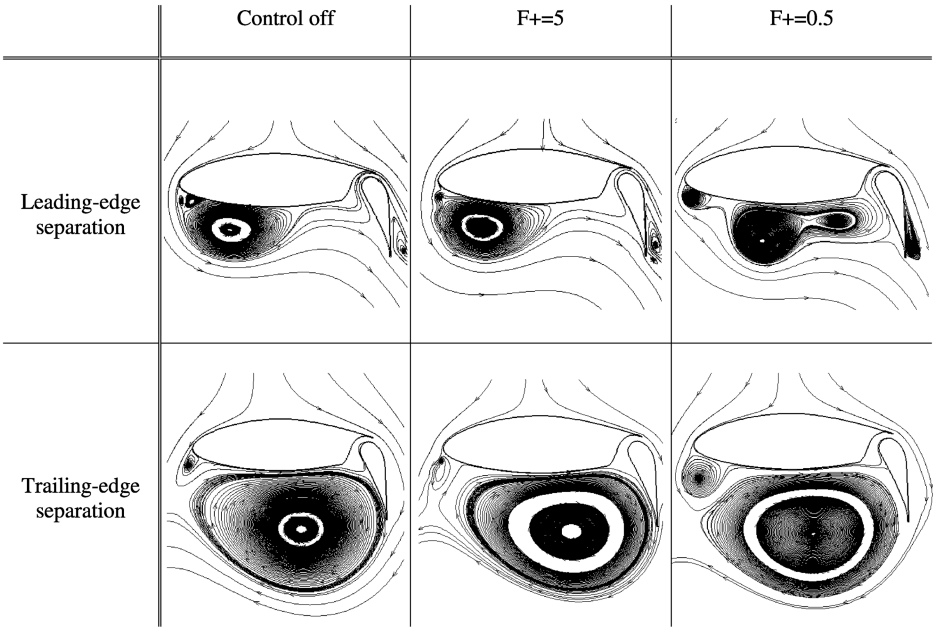

Fig. 18 Flow pattern of SUAV airfoil under leading-edge flow control in hover.

small vortices, which results in a mild increase of the drag. For interval 2, the small vortices are gradually merged to form a larger vortex, and it detaches from the airfoil after a short stay. Thus, the drag is decreased. For interval 3, almost simultaneously, the split leading-edge vortices, before they merge into a larger vortex, disturb the flow near the flap lower surface and interfere with the attachment of the trailing-edge separation vortex. Thus, the drag coefficient is not drastically increased. For interval 4, the reduced flap trailing-edge vortex is finally detached, and the drag is decreased.

Figure 20 shows the rate of drag reduction when the flow control is conducted by the leading-edge synthetic jet. As explained, the jet performance is roughly inversely proportional to the jet frequency. The wing download is reduced by about 18% at $F+ = 0.5$.

c. Trailing-Edge and Leading-Edge Separation Control. With the leading-edge and trailing-edge synthetic jets ($0.01c$, $0.3c_{\text{flap}}$, and $0.95c_{\text{flap}}$ jets), flow controls of the leading-edge and trailing-edge separation vortices were carried out. Table 3 summarizes the jet operation conditions. Based on the results of the leading-edge and trailing-edge separation controls, two cases (cases 1 and 2) with a standard operation condition ($F+ = 1$ for all jets) and two cases (cases 3 and 4) with an optimal operation condition ($F+ = 0.5$ for the $0.01c$ jet, $F+ = 5$ for the $0.3c_{\text{flap}}$ and $0.95c_{\text{flap}}$ jets) are considered. Figure 21 shows the drag histories for each case. As expected, flow control on both edges clearly yields a better performance than just the leading-edge or trailing-edge separation control. In particular, the most effective performance is case 4 ($F+ = 0.5$ for the $0.01c$ jet and $F+ = 5$ for the $0.95c_{\text{flap}}$ jet), which is consistent with the previous flow control results. Figure 22 shows the rate of drag reduction for each case. All four cases provide quite impressive performances, especially case 4, which reduces the wing download more than 40%.

Through the analyses on the leading-edge and trailing-edge separation control performance, it is observed that synthetic jet under suitable actuating conditions beneficially changes the local flow feature and vortex structure to bring a significant reduction of the wing download acting on the SUAV airfoil in the hovering flight mode.

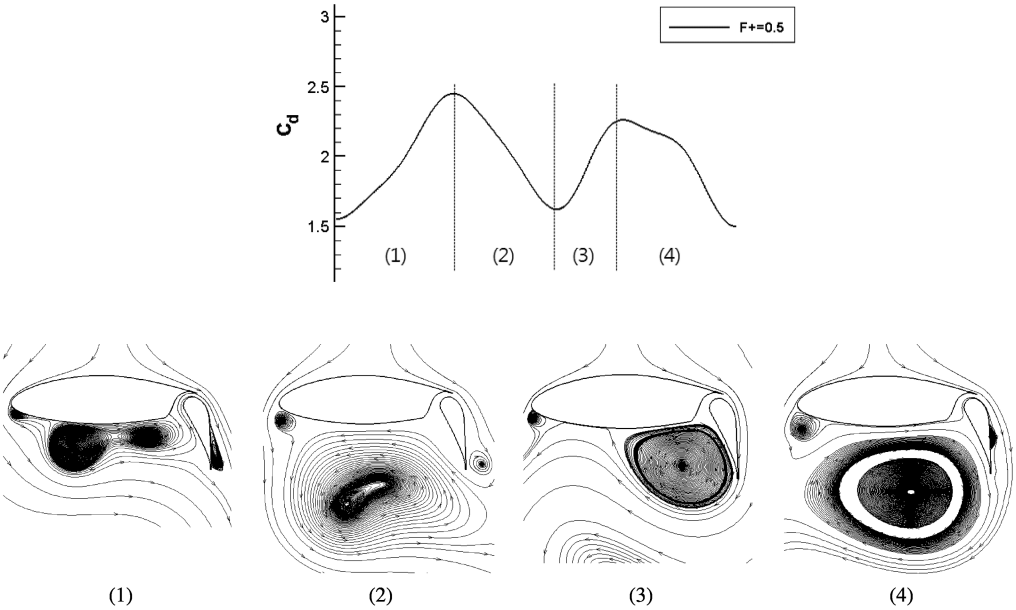

Fig. 19 Flow pattern according to drag history under leading-edge flow control in hover ($0.01c$, $F+ = 0.5$).

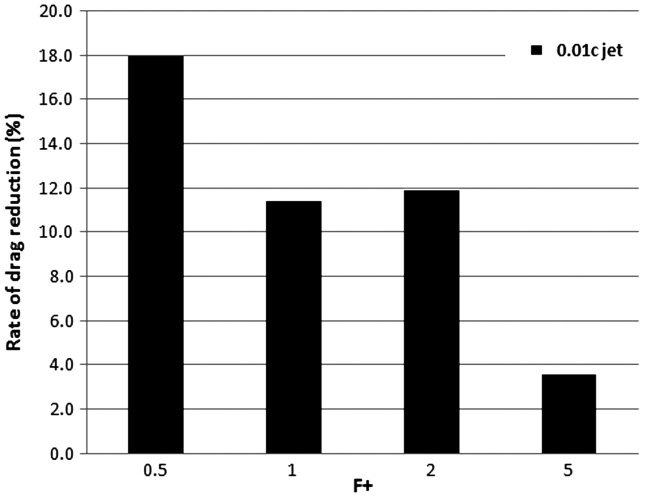

Fig. 20 Rate of drag reduction in terms of nondimensional frequency (flow control in hover, 0.01*c* jet).

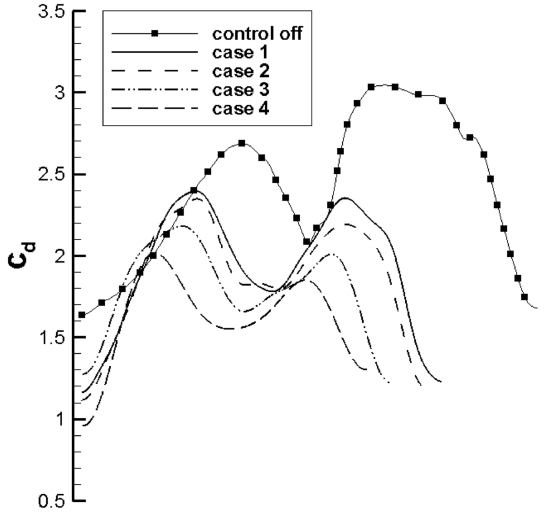

Fig. 21 Drag histories under leading-edge and trailing-edge flow controls in hover.

2. Flow Control in Transition-Flight Modes

Based on the results in the hovering flight mode, flow control in the transition flight modes was also conducted. The flow pattern in the transition flight modes changes according to the tilt angle and flap angle. As the direction of the freestream velocity is progressively horizontal, the separated flow at the leading edge becomes a dominant factor in increasing the wing download. From hovering to transition, the horizontal component of the freestream velocity gradually increases and the flap angle become smaller to avoid massive flow separation on the flap upper surface. For flow control in the transition flight modes, a synthetic jet was selected by referring the flow control results in the hovering flight mode: the $0.01c$ jet with $F+ = 0.5$ for the leading-edge synthetic jet, and the $0.95c_{\text{flap}}$ jet with $F+ = 5$ for the trailing-edge synthetic jet. The flow control performance and the rate of drag reduction were then examined in transition flight modes 1–4. Modes 5–6 were not included, since the pattern of the drag fluctuation was different from other modes (see Fig. 5); thus, the effect of flow control was not visible. This, however, does not mean the synthetic jet is not effective at all to modes 5–6. Although not included, a satisfactory flow control performance could be obtained by changing the location of the synthetic jet.

In transition flight mode 1, the tilt angle is 90° and the flap angle is 50°. The leading-edge and trailing-edge synthetic jets are applied, respectively, to control separation vortices, and the drag histories are as shown in Fig. 23. While, in the hovering flight mode, the high-frequency trailing-edge jet disturbs the separated flow on the flap upper surface and controls the flap trailing-edge flow structure, its role in transition flight mode is not visible. This is because separated flow on the flap upper surface is less dominant as the magnitude of the freestream velocity and the flap angle change (see Table 2). On the other hand, the leading-edge jet vortices efficiently prevent the leading-edge separation vortex from staying longer at the lower surface of the airfoil. In transition flight mode 1, the effect of the leading-edge synthetic jet is much more significant and the role of the flap trailing-edge jet is relatively minor. Figure 23 shows the drag history and flow structure with the leading-edge jet only, in which the overall flow structure is more or less similar to the hovering flight mode.

Table 3 Operating conditions of leading-edge and trailing-edge synthetic jets

Case	Jet conditions
1	$0.01c(F+ = 1) + 0.3c_{\text{flap}}(F+ = 1)$
2	$0.01c(F+ = 1) + 0.95c_{\text{flap}}(F+ = 1)$
3	$0.01c(F+ = 0.5) + 0.3c_{\text{flap}}(F+ = 5)$
4	$0.01c(F+ = 0.5) + 0.95c_{\text{flap}}(F+ = 5)$

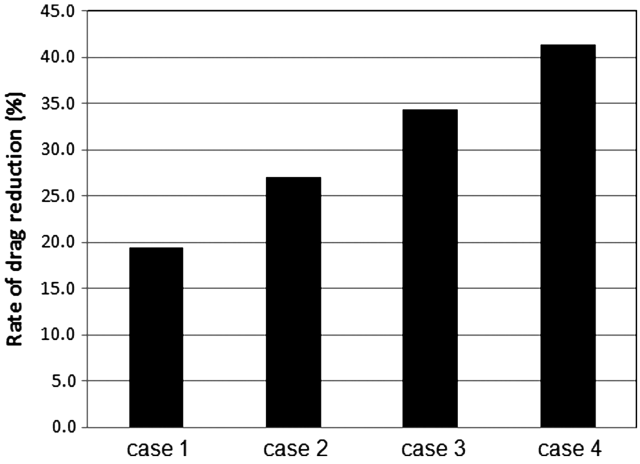

Fig. 22 Rate of drag reduction in terms of leading-edge and trailing-edge jet conditions in hover.

Transition flight mode 2, as shown in Fig. 24, also exhibits the feature that only the leading-edge synthetic jet prevails in determining the wing download characteristic. The split small vortices owing to the leading-edge jet readily move into the freestream direction, which eventually pushes the flap trailing-edge separation vortex into the freestream direction. As a result, the trailing-edge separation vortex does not stay on the flap lower surface and the period of the drag history is halved. In other words, the second drag peak that is produced by the flap trailing-edge separation vortex does not appear any longer. Figure 24 shows overall flow structure with the leading-edge synthetic jet in transition flight mode 2. The small leading-edge separation vortex is formed (interval 1) and continues to grow in size (interval 2), which leads to the steady drag increase in intervals 1–2. The fully developed leading-edge separation vortex is then detached. The trailing-edge separation vortex is developed, but it does not stay close to the flap surface (interval 3), and it finally moves away into the freestream direction (interval 4). As a result, the drag is steadily decreased in intervals 3–4.

The freestream velocity component is increasing in transition flight modes 3–4; thus, the flow control characteristic observed in mode 2 is accentuated. Figures 25 and 26 show the reduction of the effective download by applying the leading-edge synthetic jet only. Flow structures similar to transition flight mode 2 are shown in Figs. 24, but the size and intensity of the flap separation vortex become weaker. Figure 27 shows the rate of drag reduction in all the transition flight modes and it confirms again that efficient flow

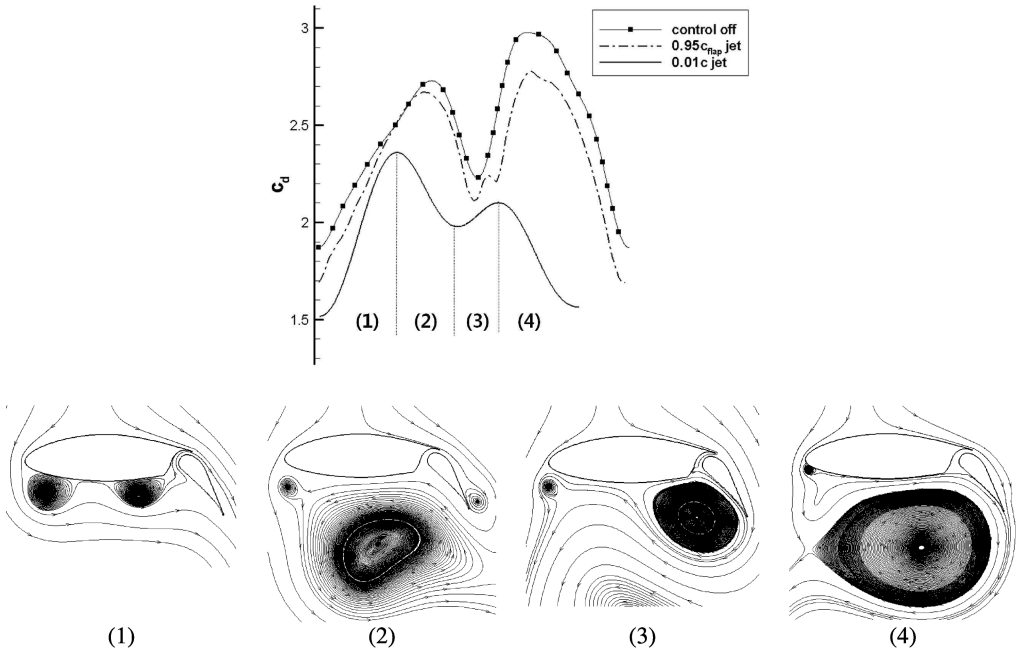

Fig. 23 Drag histories and flow pattern under leading-edge flow control in transition flight mode 1 (0.01c jet, $F+ = 0.5$).

control can be realized by operating the leading-edge synthetic jet only. With the leading-edge synthetic jet of $F+ = 0.5$, drag can be reduced from 6 to 58%. In mode 4, the flow control effect is not substantial compared with other modes. This is partially because the jet location and jet angle may not be optimal, and the amplitude of the drag fluctuation is relatively smaller.

Figure 28 summarizes the results of separation control using synthetic jets. The leading-edge jet with low frequency and the trailing-edge jet with high frequency are most effective in the hovering flight mode. In addition, the leading-edge jet with low frequency, operated in all transition-flight modes, is quite effective. The wing download is reduced in both the hovering and transition flight modes. The rate of the drag reduction is about 43% in hover, and in transition flight modes, the drag can be reduced up to about 58%. Consequently, the flight performance of the SUAV can be remarkably improved, both in hovering and transition flight modes, by the proposed flow control strategy based on synthetic jets.

V. Conclusions

To reduce the download on the wing produced by the rotor-induced downwash of a tiltrotor UAV, flow structures in the hovering and transition flight modes were analyzed, and flow control using synthetic jets was then conducted. Through analyses of the computed flowfields in the hovering and transition flight modes, it is observed that the wing download is determined by the growth and detachment of the leading-edge and flap trailing-edge vortices. In the hovering flight mode, the leading-edge and flap trailing-edge vortices are equally influential. In the transition flight mode, however, flow structure becomes more dependent on the evolution of the leading-edge vortex. Exploiting the observed flow characteristics, leading-edge and trailing-edge separation controls are carried out by suitably positioned synthetic jets.

Flow control in hover was achieved by applying the leading-edge and trailing-edge synthetic jets. Detailed numerical simulations suggest that a high-frequency jet at the trailing edge efficiently suppresses the generation of the flap trailing-edge separation vortex.

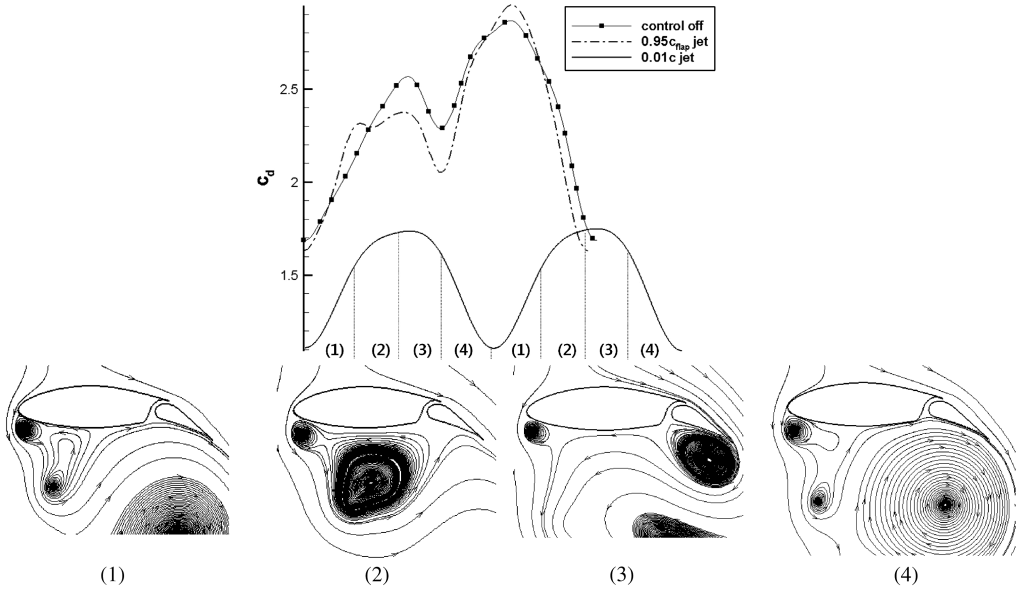

Fig. 24 Drag histories and flow pattern under leading-edge flow control in transition flight mode 2 (0.01c jet, $F+ = 0.5$).

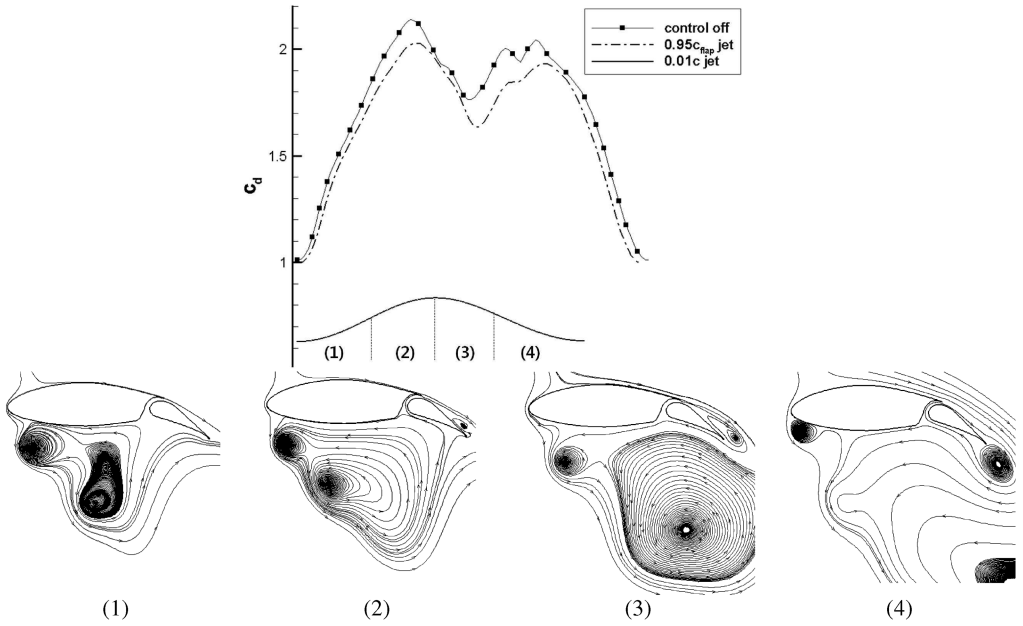

Fig. 25 Drag histories and flow pattern under leading-edge flow control in transition flight mode 3 (0.01c jet, $F+ = 0.5$).

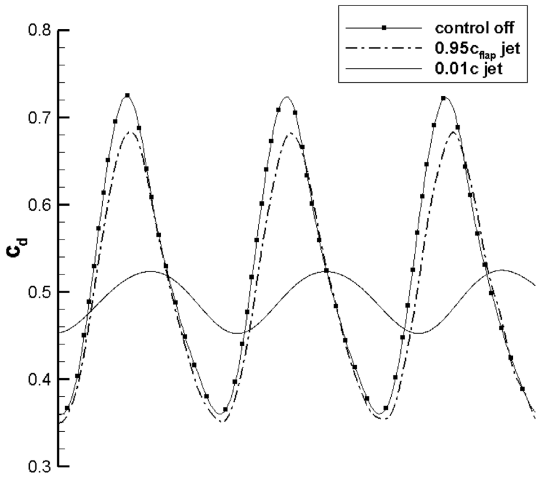

Fig. 26 Drag histories under flow control in transition flight mode 4.

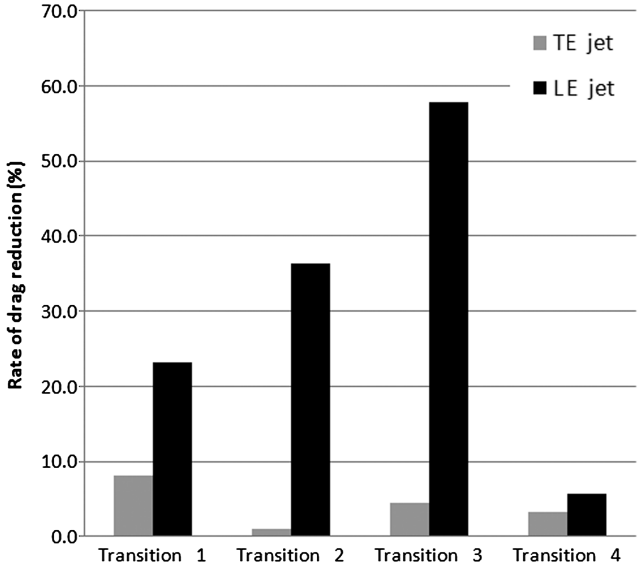

Fig. 27 Rate of drag reduction in transition flight modes (TE denotes trailing edge, and LE denotes leading edge).

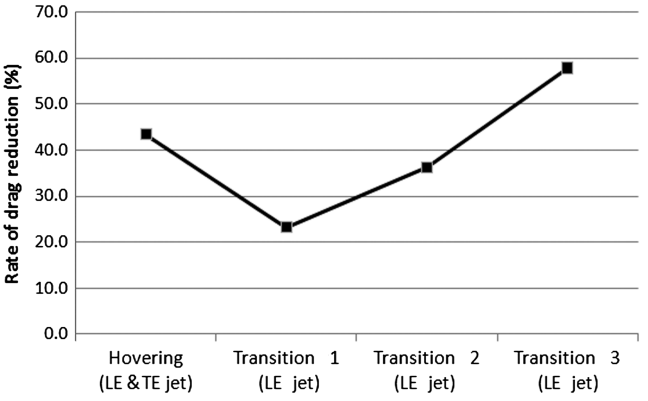

Fig. 28 Rate of drag reduction in hovering and transition-flight conditions (TE denotes trailing edge, and LE denotes leading edge).

Vortices produced by the leading-edge jet continuously disturb the large leading-edge separation vortex and finally split it into smaller vortices. Flow control effect was most visible with the low-frequency leading-edge jet. With both the low-frequency leading-edge and high-frequency trailing-edge synthetic jets (the $0.01c$ jet with $F+ = 0.5$, and the $0.95c_{\text{flap}}$ jet with $F+ = 5$), the wing download in hover was significantly reduced more than 40%.

The outcome of the flow control strategy in hover was extended to control separation vortices in the transition flight modes. It is observed that the leading-edge separation flow is a dominant factor in increasing the transition download; thus, the role of the leading-edge synthetic jet is much more significant in determining overall flow structures. Efficient flow control in all transition modes is possible with the leading-edge jet only. By operating the low-frequency leading-edge synthetic jet only (the $0.01c$ jet with $F+ = 0.5$), drag can be remarkably reduced.

Based on the numerical results and comparisons, it is observed that the wing loading on the SUAV can be significantly reduced by applying the proposed flow control strategy using synthetic jets.

Acknowledgments

This research was supported by the Korea Science and Engineering Foundation grant funded by the Korean government's Ministry of Education, Science, and Technology (MEST) (No. 20090084669),

National Space Laboratory program through the National Research Foundation of Korea funded by the MEST (grant 20090091724) and Defense Acquisition Program Administration and Agency for Defense Development (UC100031JD). The authors also appreciate the financial and administrative help from the Institute of Advanced Aerospace Technology.

References

[1] Fejtek, I. G., "Navier–Stokes Flowfield Computation of Wing/Rotor Interaction for a Tilt Rotor Aircraft in Hover," NASA TM 02-185011, 1993.

[2] Maisel, M., and Harris, D., "Hover Tests of the XV-15 Tilt Rotor Research Aircraft," AIAA SETP/SFTE/SAE/ITEA/IEEE 1st Flight Test Conference, Las Vegas, NV, AIAA Paper 1981-2501, 1981.

[3] McCroskey, W., Spalart, P., Laub, G., Maisel, M., and Maskew, B., "Airloads on Bluff Bodies, with Application to the Rotor-Induced Downloads on Tilt-Rotor Aircraft," *Vertica*, Vol. 9, No. l, 1985, pp. 1–11.

[4] Felker, F. F., "A Review of Tilt/Rotor Download Research," *14th European Rotorcraft Forum*, Milan, No. 14, Italian Assoc. of Aeronautics and Astronautics, Rome, 1988, pp. 1–33.

[5] McVeigh, M. A., Nagib, H., Wood, T., Kiedaisch, J., Stalker, A., and Wygnanski, I., "Model and Full Scale Tilt-Rotor Download Reduction Tests Using Active Flow Control," *AHS 60th Annual Forum*, Baltimore, MD, American Helicopter Soc. International, Gardena, CA, 7–10 June 2004.

[6] Nagib, H., Kiedaisch, J., Stalker, A., Wygnanski, I., McVeigh, M. A., and Wood, T., "First-In-Flight Full-Scale Application of Active Flow Control: The XV-15 Tilt-Rotor Download Reduction," *NATO Research and Technology Specialists' Meeting*, Prague, NATO RTO-MP-AVT-111, Oct. 2004.

[7] Grife, R., Darabi, A., and Wygnanski, I., "Download Reduction on a Three Dimensional V-22 Model Using Active Flow Control," 1st Flow Control Conference, St. Louis, MO, AIAA Paper 2002-3071, June 2002.

[8] Kjellgren, P., Anderberg, N., and Wygnanski, I., "Download Alleviation by Periodic Excitation on a Typical Tilt-Rotor Configuration," FLUIDS 2000 Conference and Exhibit, Denver, CO, AIAA Paper 2000-2697, June 2000.

[9] Fejtek, I., and Roberts, L., "Navier–Stokes Computation of Wing Leading Edge Tangential Blowing for a Tilt-Rotor in Hover," 10th AIAA Applied Aerodynamics Conference, Palo Alto, CA, AIAA Paper 1992-2608, June 1992.

[10] Spalart, P., Hedges, L., shur, M., and Travin, A., "Simulation of Active Flow Control on a Stalled Airfoil," *Flow, Turbulence and Combustion*, Vol. 71, Nos. 1–4, 2003, pp. 1573–1987. doi:10.1023/B:APPL.0000014925.91304.42

[11] Vasile, J., Elimelech, Y., Farnsworth, J., and Amitay, M., "Interaction of a Finite-Span Synthetic-Jet and Cross-Flow over a Swept Wing," 5th Flow Control Conference, Chicago, IL, AIAA Paper 2010-4584, July 2010.

[12] Vaccaro, J. C., Gressick, W., Wen, J., and Amitay, M.,"An Experimental Investigation of Flow Control Inside Inlet Ducts," 47th AIAA Aerospace Sciences Meeting Including the New Horizons Forum and Aerospace Exposition, Orlando, FL, AIAA Paper 2009-0740, Jan. 2009.

[13] Kim, S. H., and Kim, C., "Separation Control on NACA23012 Using Synthetic Jet," *Aerospace Science and Technology*, Vol. 13, Nos. 4–5, June–July 2009, pp. 172–182. doi:10.1016/j.ast.2008.11.001

[14] Kim, W., Kim, S., Choi, K., and Kim, C., "Experimental and Computational Study on Flow Characteristics by Synthetic Jets Configuration," 48th AIAA Aerospace Sciences Meeting Including the New Horizons Forum and Aerospace Exposition, Orlando, FL, AIAA Paper 2010-864, Jan. 2010.

[15] Xia, X., Mohseni, K., "Modeling and Experimental Investigations of Synthetic Jet in Cross-Flow," 48th AIAA Aerospace Sciences Meeting Including the New Horizons Forum and Aerospace Exposition, Orlando, FL, AIAA Paper 2010-106, Jan. 2010.

[16] Mohseni, K., "Pulsating Vortex Generators for Low-Speed Maneuvering of Small Underwater Vehicles," *Ocean Engineering*, Vol. 33, No. 16, Nov. 2006, pp. 2209–2223. doi:10.1016/j.oceaneng.2005.10.022

[17] Chaudhari, M., Vermaa, G., Puranika, B., and Agrawal, A.,"Frequency Response of a Synthetic Jet Cavity," *Experimental Thermal and Fluid Science*, Vol. 33, No. 3, March 2009, pp. 439–448. doi:10.1016/j.expthermflusci.2008.10.008

[18] Chaudhari, M., Puranik, B., and Agrawal, A., "Effect Of Orifice Shape in Synthetic Jet Based Impingement Cooling," *Experimental Thermal and Fluid Science*, Vol. 34, No. 2, Feb. 2010, pp. 246–256. doi:10.1016/j.expthermflusci.2009.11.001

[19] Zhou, J., and Zhong, S., "Numerical Simulation of the Interaction of a Circular Synthetic Jet with a Boundary Layer," *Computers and Fluids*, Vol. 38, No. 2, 2009, pp. 393–405. doi:10.1016/j.compfluid.2008.04.012

[20] Zhou, J., and Zhong, S., "Coherent Structures Produced by the Interaction Between Synthetic Jets and a Laminar Boundary Layer and Their Surface Shear Stress Patterns," *Computers and Fluids*, Vol. 39, No. 8, 2010, pp. 1296–1313. doi:10.1016/j.compfluid.2010.04.001

[21] Wood, J., Sahni, O., Jansen, K., and Amitay, M., "Experimental and Numerical Investigation of Active Control of 3-D Flows," 39th AIAA Fluid Dynamics Conference, San Antonio, TX, AIAA Paper 2009-4279, June 2009.

[22] Günther, B., Thiele, F., Petz, R., Nitsche, W., Sahner, J., Weinkaufk, T., and Hege, H.-C., "Control of Separation on the Flap of a Three-Element High-Lift Configuration," 45th AIAA Aerospace Sciences Meeting and Exhibit, Reno, NV, AIAA Paper 2007-0265, Jan. 2007.

[23] Petz, R., and Nitsche, W., "Active Separation Control on the Flap of a Two-Dimensional Generic High-Lift Configuration," *Journal of Aircraft*, Vol. 44, No. 3, May–June 2007, pp. 865–874. doi:10.2514/1.25425

[24] Rumsey, C. L., Gatski, T. B., Seller, W. L., III, Vasta, V. N., and Viken, S. A., "Summary of the 2004 CFD Validation Workshop on Synthetic Jets and Turbulent Separation Control," 2nd AIAA Flow Control Conference, Portland, OR, AIAA Paper 2004-2217, June 2004.

[25] Chorin, A. J., "A Numerical Method for Solving Incompressible Viscous Flow Problems," *Journal of Computational Physics*, Vol. 2, No. 1, Aug. 1967, pp. 12–26. doi:10.1016/0021-9991(67)90037-X

[26] Kim, C. S., Kim, C., and Rho, O. H., "Parallel Computations of High-Lift Airfoil Flows Using Two-Equation Turbulence Models," *AIAA Journal*, Vol. 38, No. 8, 2000, pp. 1360–1368. doi:10.2514/2.1135

[27] Yoon, S., and Kwak, D., "Three-Dimensional Incompressible Navier–Stokes Solver Using Lower-Upper Symmetric Gauss Seidel Algorithm," *AIAA Journal*, Vol. 29, No. 6, 1991, pp. 874–875. doi:10.2514/3.10671

[28] Bardina, J. E., Huang, P. G., and Coakley, T. J.,"Turbulence Modeling Validation, Testing and Development," NASA TM 110446, April 1997.

[29] Zheng, X., Liu, C., Liu, F., and Yang, C., "Turbulent Transition Simulation Using the k-ω model," *International Journal for Numerical Methods in Engineering*, Vol. 42, No. 5, 1998, pp. 907–926. doi:10.1002/(SICI)1097-0207(19980715)42:5<907::AID-NME393>3.0.CO;2-T

[30] Kim, C. S., Kim, C., and Rho, O. H., "Sensitivity Analysis for the Navier–Stokes Equations with Two-Equation Turbulence Models," *AIAA Journal*, Vol. 39, No. 5, 2001, pp. 838–845. doi:10.2514/2.1387

[31] Rumsey, C. L., "Computation of a Synthetic Jet in a Turbulent Cross Flow Boundary Layer," NASA TM 213273, 2004.

[32] Kral, L. D., Donovan, J. F., Cain, A. B., and Cary, A. W., "Numerical Simulation of Synthetic Jet Actuators," 4th AIAA Shear Flow Control Conference, Snowmass Village, CO, AIAA, Paper 1997-1824, 1997.

[33] Duvigneau, R., and Visonneau, M., "Optimization of a Synthetic Jet Actuator for Aerodynamic Stall Control," *Computers and Fluids*, Vol. 35, No. 6, July 2006, pp. 624–638. doi:10.1016/j.compfluid.2005.01.005

[34] Yao, C., Chen, F. J., and Neuhart, D., "Synthetic Jet Flowfield Database for Computational Fluid Dynamics Validation," *AIAA Journal*, Vol. 44, No. 12, 2006, pp. 3153–3157. doi:10.2514/1.13819

[35] Choi, S. W., and Kim, J. M., "Unsteady Flow Simulation for Powered Tilt Rotor UAV," KSCFE Spring Conference 2007, Korean Soc. of Computational Fluids Engineering, Seoul, ROK, 2007, pp. 8–13.

[36] Gallas, Q., Holman, R., Nishida, T., Carroll, B., Sheplak, M., and Cattafesta, L., "Lumped Element Modeling of Piezoelectric-Driven Synthetic Jet Actuators," *AIAA Journal*, Vol. 41, No. 2, 2003, pp. 240–247. doi:10.2514/2.1936

[37] McCormick, D. C., Lozyniak, S. A., MacMartin, D. G., and Lorber, P. F., "Compact, High-Power Boundary Layer Separation Control Actuation Development," 2001 ASME Fluids Engineering Division Summer Meeting, New Orleans, LA, American Soc. of Mechanical Engineers Paper 18279, Fairfield, NJ, June 2001.